RACH Performance Analysis for Large-scale Cellular IoT Applications

Hesham G. Moussa, *Student Member, IEEE,* Weihua Zhuang, *Fellow, IEEE,*

***Abstract*—Providing energy efficient and delay-aware access is essential to many anticipated cellular Internet of Things (IoT) applications. In cellular networks, before devices transmit their data, they use a contention-based association protocol, known as RACH, which introduces extensive access delays and energy wastage as the number of contending devices increases. Modeling the performance of the RACH protocol is a challenging task due to the complexity of uplink transmission that exhibits a wide range of interference components; nonetheless, it is an essential process that will help determine the applicability of cellular IoT communication paradigm. This paper presents a novel mathematical framework based on stochastic geometry to analyze the RACH protocol and identify its limitations in the context of cellular IoT applications with a massive number of devices. To do so, we study the traditional cellular association process and derive a mathematical model for its association success probability. The derived model accounts for device density, spatial characteristics of the network, power control employed, and mutual interference among the devices. Our analysis and results highlight the shortcomings of the RACH protocol and give insights into the potentials brought on by employing power control techniques. The developed framework can be applied to evaluate the performance of other contention-based access schemes by incorporating their unique operational principles.**

***Index Terms*—massive machine communications, RACH protocol, stochastic geometry, uplink modeling, cellular network, Internet of Things.**

I. Introduction

THE Internet of Things (IoT) is expected to have a high impact on various aspects of everyday-life, as it will help realize many intelligent applications such as environmental monitoring, smart cities, intelligent transport systems, and e-health applications. To many of these applications, energy efficiency and timeliness in information delivery are crucial aspects to their success [1]. However, with the proliferation in IoT applications, a large network that is made up of a massive number of heterogeneous devices spread across a large surface area will be formed. Such unconventional network brings many new networking challenges that have attracted attentions from many researchers in recent years.

According to various standardization bodies, IoT will become an important source of traffic in future 5G networks [2]. Among various proposed 5G technologies, densified cellular networks are considered to be the most suitable access network, thanks to their wide coverage area, high device capacity, low device energy consumption and mobility support features. In traditional cellular communication, for a device to transmit its data, it has to first go through an association process that is done over the physical random access channel (PRACH). According to the 3^{rd} Generation Partnership Project (3GPP), the number of IoT devices in the coverage range of a typical base station (BS) is expected to exceed thirty thousand devices. Due to the random access nature of the association process, with a such large number of contending devices, a massive number of simultaneous access requests will be generated, resulting in the congestion of the PRACH. A congested PRACH introduces sensible network access delays, increases device energy consumption, and reduces network good-put [3]. Therefore, to provide ubiquitous energy efficient and timely connectivity, improving network access is crucial [4]. Yet, the solution should be economically viable and comes at minimum infrastructural alteration [3], [5].

In current cellular communication, devices use a contention-based 4-way handshake procedure, known as the random access channel protocol (RACH), to associate with their desired BSs over the PRACH. In the first step of the RACH protocol, an active device, with data to transmit, randomly chooses and transmits a preamble to its desired BS. The 3GPP defines a fixed set of orthogonal preambles which is shared by all the devices in the network. Thus, as the number of contending devices increases, the possibility of more than one device in a cell choosing the same preamble simultaneously increases, leading to extensive access delays and elevated levels of energy consumption [6]. This problem is known as the PRACH overload problem and has been well studied in the literature. In fact, many of the proposed solutions have already been implemented in the current cellular access network for the purpose of alleviating congestion and enhancing system throughput [3], [5]. However, these solutions are yet to be optimized for massive access scenarios such as IoT applications.

Thus, as a step towards improving the performance of the cellular access network when supporting large-scale IoT applications, many researchers have studied the RACH protocol and modeled its performance under massive access setting [3], [7]–[9]. Most of these studies are based on the assumption that all colliding devices will be denied access and have to reattempt the RACH protocol in subsequent opportunities [3]. While this assumption is valid, with the recent improvements in the computational abilities of BSs and the introduction of various multi-user detection techniques, it becomes possible

Manuscript submitted for review on September 20, 2018. This work was supported by the Natural Sciences and Engineering Research Council (NSERC) of Canada (NSERC Canadian FloodNet).

The authors are with the Department of Electrical and Computer Engineering, University of Waterloo, Waterloo, ON N2L 3G1, Canada (e-mail: h3moussa@uwaterloo.ca; wzhuang@uwaterloo.ca)

for colliding devices to successfully associate if their preambles are received with the signal to interference plus noise ratio (SINR) above a certain threshold [10]. Accordingly, many of the widely accepted solutions for the PRACH overload problem, such as access class baring (ACB) [3], enhanced access barring (EAB) [5], data aggregation [11], and user association [12], can be further optimized to yield improved RACH association performance suitable for future large-scale IoT applications [13]. Therefore, to investigate the RACH performance under this new scenario, novel SINR models are needed to capture the added complexity due to multi-user detection.

In the RACH protocol, devices randomly choose and transmit their preambles to their desired BSs. Devices transmitting the same preamble simultaneously interfere with each other. The interference is a function of the power of transmitted preambles by all interfering devices. In wireless networks, the power of a transmitted signal experiences attenuation that increases with the propagation distance. Since the preambles are chosen randomly, this creates a random set of interfering devices on a preamble with random propagation distances among them. Capturing the randomness in the propagation distances among interfering devices is crucial for accurately modeling the SINR of the RACH protocol. Therefore, the spatial characteristics of the network plays an important role in determining the SINR of any received preamble in the network and shall be taken into consideration when evaluating performance of the RACH protocol.

For many years, stochastic geometry has been used to study the performance of different complex wireless networks such as mobile ad hoc networks, wireless sensor networks, and heterogeneous cellular networks [14]. By combining theories from various fields such as principles of geometry, probability theory, stochastic processes, percolation theory, information theory, and Fourier analysis, stochastic geometry presents a powerful modeling tool for developing tractable statistical models that take into consideration the spatial characteristics of the network. Motivated by its unique characteristics, in recent years, researchers have used stochastic geometry to study the performance of the RACH protocol with multi-user detection in a full- power inversion situation where interfering devices fully compensated for the path-loss attenuation experienced [10], [15], [16]. These works lay the ground for developing a mathematical model for the RACH performance, and further research is required to model the SINR in the RACH protocol in a more general manner.

In an attempt for developing a more comprehensive model that takes into account various system variables, in this paper, we use stochastic geometry to analyze the association success probability of the RACH protocol in a large-scale single-tier cellular network that supports a large number of identical IoT devices. Inspired by the methodology in [17], we consider fractional power control (FPC) and biased device association. The main contributions of this work are summarized as follows:

- We present a novel mathematical framework for modeling the performance of the RACH protocol under large-scale IoT applications. We model the SINR of the preamble transmission and derive an expression for the instantaneous association success probability;
- The developed model is comprehensive as it accounts for various network parameters including device density, spatial spread of the network, channel characteristics, association policy, device power control, and the number of available preambles. The model highlights the effect of both intra-cell and inter-cell interference factors on the success probability;
- The accuracy of the analytic model is corroborated via computer simulations;
- The joint effect of the FPC, device density, and the SINR threshold on the success probability is studied and the main trade-offs are highlighted.

The rest of this paper is structured as follows. In Section II, we describe the system model under consideration. In Section III, the spatial characteristics of the network are used to characterize the interference components in the network. Section IV presents a step-by-step derivation of the association success probability for the RACH protocol. Section V discusses the numerical and simulation results and summarizes the main findings. This study is then concluded in Section VI.

II. System Model

In this section, we first describe the spatial characteristics of the network under consideration, and briefly summarize the RACH association process and the collision process among contending devices. The physical channel model is then introduced with details on the power control mechanism employed by the devices in the network. The main notations and symbols are listed in Table I.

A. Spatial description

Consider a large-scale single-tier cellular network with identical BSs that are spatially distributed in $\mathbb{R}^2$ according to a Poisson point process (PPP) $\Phi = \{b_0, b_1, b_2, ...\}$ with device density λ_B where b_j denotes the 2D location of the j^{th} BS. The network supports a massive number (Ω) of stationary identical devices that are uniformly distributed across the plane. Devices can be in one of two states: active or inactive. An inactive device has no data to transmit, and stays in the sleep mode in which it switches off its communication module to save energy. Inactive devices are not associated with any BS. Once a device has data to transmit, its state changes from inactive to active. It then attempts to associate with its desired BS according to the maximum received signal strength (max-RSS) association rule. A device receives orthogonal preamble messages from multiple BSs. It decodes the preambles, determines the ID of each BS, and measures the downlink received power from each. It then starts the association process with the BS from which it received the highest downlink power [18]. Devices are allowed to associate with only one BS at a time. Once a device completes its data transmission, it switches off its communication module and terminates the BS association; thus, new association is needed every time that a device has data to transmit.

TABLE I. Notation Table

Parameter	Description
τ	SINR threshold
ϵ	Fractional power control factor
α	Path-loss attenuation factor
g	Channel gain
ρ	Receiver sensitivity of any device
P	Nominal transmission power of any device
λ_B	Density of BSs
λ_u	Density of active devices at the beginning of a transmission round
λ_n	Density of interfering devices on the n^{th} preamble
N	Number of available preambles
b_j	2D location of the j^{th} BS
u_i	2D location of the i^{th} device
u_i^n	2D location of the i^{th} interfering device on the n^{th} preamble
u_{ji}^n	2D location of the i^{th} interfering device associated with the j^{th} BS
Φ	Poisson point process of BSs
Ψ	Poisson point process of active devices
Ψ_n	Poisson point process of interfering devices
Ψ_{nj}	location set of interfering devices associated with the j^{th} BS
BS_0	Denotes the typical BS
device_0	Denotes the typical device
Θ_{ji}^n	SINR of the n^{th} preamble transmitted by the i^{th} device and received by the j^{th} BS
Q_{ji}^n	Association success probability
I_{in}	Intra-cell interference component
I_{out}	Inter-cell interference component
R_{0i}^n	Distance between i^{th} device located inside the Voronoi cell of BS_0 and the origin
Y_{ji}^n	Distance between the i^{th} device, associated with the j^{th} BS (for $j > 0$), and its serving BS
X_{ji}^n	Distance between the i^{th} device, associated with the j^{th} BS (for $j > 0$), and the origin
$\bar{M}$	Number of intra-cell interfering devices on any preamble

Time is divided into equal transmission frames, referred to as *rounds*, each of length T, as shown in Figure 1. Each *round* is divided into f sub-frames, and each sub-frame has two slots: a random access opportunity (RAO) and a transmission period. A batch of devices becomes active at the beginning of each *round*. Active devices are spatially distributed according to a PPP $\Psi = \{u_1, u_2, ...\}$ with device density λ_u ($>> \lambda_B$) where u_i denotes the 2D location of the i^{th} active device. A *round* is sufficiently long such that there will be no backlogged data at the devices from previous *rounds*.

A device goes through two stages before it successfully completes its data transmission [3], [19]. The first stage is the association stage where the RACH protocol is invoked and it takes place during the RAO slot of a sub-frame. The second stage is the transmission stage which takes place during the transmission slot of a sub-frame. In the transmission stage, successfully associated devices are allocated orthogonal resources over which they transmit their data [19]. Here we give a brief description of the first stage.

Every time a device becomes active, it uses the RACH protocol to associate with a BS [3], [19]. In the first step of the RACH, a device randomly chooses (generates) a preamble and transmits it to its desired BS on the shared PRACH. In response, in the second step of the RACH protocol, the BS broadcasts a random access response (RAR) message that consists of the detected preamble index corresponding

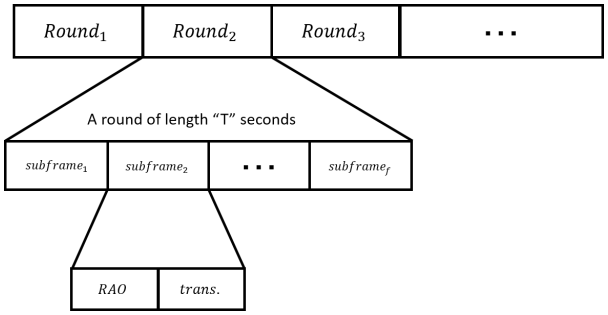

Fig. 1: Channel access time frame structure

to the sequence sent by the device, along with other control information. In the third step, the device uses the control information in the received RAR to synchronize with the BS and awaits its dedicated uplink resource blocks (RBs) on the physical uplink control channel. In the dedicated RBs, the device transmits a connection request using a radio resource control message which contains identity information as well as the amount of uplink resources required for it to transmit its payload. If the control message is successfully received by the BS, an acknowledgment is sent to the transmitting device indicating the assigned uplink orthogonal resources. Correct reception of the acknowledgement by the device successfully completes its association [19].

All devices share a fixed number of preambles, N ($<< \Omega$). All the preambles are equiprobable to be selected, each with probability $\beta = 1/N$. Preambles are transmitted in broadcast manner and thus are heard by all nearby BSs in the network. Therefore, all devices choosing the same preamble and transmitting at the same time will interfere with each other at their respective desired BSs. A device can successfully associate with its desired BS, if its preamble is received with SINR above a threshold τ at the BS. In Section III, we characterize the SINR in the network in details.

B. Transmission model

Transmitted signals in both uplink and downlink experience propagation attenuation according to a general power-law path-loss model. The signal power decays at rate $D^{-\alpha}$, where D is the propagation distance and α is the path-loss exponent. Consider a Rayleigh fading channel that introduces a random instantaneous power gain, g, which follows an exponential distribution with unity mean (i.e. $g \sim \exp\{1\}$). Channel gains are assumed to be distance independent as well as independent of each other and identically distributed (i.i.d.). The channel also introduces additive white Gaussian noise (AWGN) with received noise power, σ^2.

Devices employ FPC mechanism by which they adjust their transmission power to compensate partially or fully for the propagation attenuation. Accordingly, denote the device transmission power before performing FPC by the nominal power, P, which is the same for all devices [20]. For a device located at u and transmitting its preamble to a BS located at b, the received power at the BS is $P_r = P||u - b||^{-\alpha} g$ in the absence of noise, where $||u-b||$ denotes the Euclidean distance

between the device and the BS. Now, using FPC, the device adjusts its transmission power such that it can compensate for the attenuation due to propagation loss. Therefore, the transmission power of the device after FPC is $P_t = P||u-b||^{\epsilon\alpha}$, where $\epsilon \in [0,1]$ is the power control factor and is a design parameter that is fixed for all devices in the network. If $\epsilon = 1$, the device achieves full power control; if $\epsilon = 0$, the device does no power control. Hence, the power received at the BS is $P_r^{FPC} = P||u-b||^{(\epsilon-1)\alpha} g$. In order for a device to transmit its signal, its maximum allowable transmission power should be high enough for the fractional path-loss compensation to be achievable. Here, as in previous studies, we do not consider the maximum transmission power limitation [17], [20].

III. SINR CHARACTERIZATION

Since the set of preambles is shared by all the BSs in the network, there are two types of interference in the network: intra-cell interference (I_{in}) and inter-cell interference (I_{out}). Intra-cell interference is due to transmissions from devices choosing the same preamble while associated with the same BS, whereas inter-cell interference is due to transmissions from devices choosing the same preamble and associated with different BSs.

Since devices choose their preambles randomly and independently, interfering devices on the n^{th} preamble can be spatially modeled by a thinned PPP $\Psi_n = \{u_1^n, u_2^n, ...\}$ with device density $\lambda_n = \beta\lambda_u$, where u_i^n denotes the location of the i^{th} device interfering on the n^{th} preamble for $n = 1, 2, ..., N$. Note that all active devices have to choose a preamble to transmit; therefore, $\Psi = \cup_{n=1}^{N} \Psi_n$. Also, let $\Psi_{nj} = \{u_{j1}^n, u_{j2}^n, ...\}$ denote the location set of intra-cell interfering devices on the n^{th} preamble and are associated with the j^{th} BS for $j = 0, 1, 2, ...$ and $n = 1, 2, ..., N$. The combination of those sets constitutes the total location set of all devices choosing the n^{th} preamble across the network (i.e. $\cup_j \Psi_{nj} = \Psi_n$)).

A. SINR mathematical representation

Without loss of generality, we focus on a typical BS and its associated typical device. The coordinates are shifted such that the BS is located at the origin (i.e., $b = (0,0)$). According to Slivnyak's theorem [21], the presented analysis can be generalized for any generic device-BS pair located anywhere in the network. Both the typical BS and the typical device are indexed by zero (i.e., $j = 0$ and $i = 0$). That is, the typical device associating with the typical BS via transmitting the n^{th} preamble is located at $u_{ji}^n = u_{00}^n$. For ease of notation, let BS_0 denote the typical BS and device_0 denote the typical device.

Now, let Θ_{ji}^n denote the SINR level of the n^{th} preamble transmitted by the i^{th} device that is associated with the j^{th} BS. Hence, for device_0 associating with BS_0, the SINR of the received preamble is given by

$$\Theta_{00}^n = \frac{P||u_{00}^n||^{(\epsilon-1)\alpha} g_0}{I_{in} + I_{out} + \sigma^2}. \tag{1}$$

In (1), I_{in} and I_{out} are given by

$$I_{in} = \sum_{u_{0i}^n \in \Psi_{n0}/\{u_{00}^n\}} P||u_{0i}^n||^{(\epsilon-1)\alpha} g_i \tag{2a}$$

$$I_{out} = \sum_{j\neq 0} \sum_{u_{ji}^n \in \Psi_{nj}} P||u_{ji}^n - b_j||^{\epsilon\alpha} ||u_{ji}^n||^{-\alpha} g_i \tag{2b}$$

where g_i is the channel gain experience by the i^{th} device, $\Psi_{n0}/\{u_{00}^n\}$ is the set of locations of intra-cell interfering devices associated with BS_0 excluding the location of device_0, $||u_{ji}^n||$ denotes the Euclidean distance between the i^{th} inter-cell interfering device and the origin, and $||u_{ji}^n - b_j||$ is the Euclidean distance between the i^{th} inter-cell interfering device and its serving BS (the j^{th} BS). Note that $||u_{00}^n||$, $||u_{0i}^n||$, $||u_{ji}^n||$, and $||u_{ji}^n - b_j||$ are all random distances as they depend on the locations of the device and the BS. In the rest of this work, these random distances are referred to as link lengths as defined below.

B. Link length characterization

A link length refers to the Euclidean distance between a device and a BS. Since devices transmit in the uplink direction in a broadcast manner, the signal from each device is received by all BSs. Therefore, there is a link length between each device and each BS in the network. These link lengths can be classified into 4 types. As shown in Figure 2, the 4 types of link lengths are: 1) between device_0 and BS_0 ($R_{00}^n = ||u_{00}^n||$), 2) between the i^{th} intra-cell interfering device and BS_0 ($R_{0i}^n = ||u_{0i}^n||$), 3) between the i^{th} inter-cell interfering device and the j^{th} BS (i.e. its serving BS) ($Y_{ji}^n = ||u_{ji}^n - b_j||$), and 4) between the i^{th} inter-cell interfering device and BS_0 ($X_{ji}^n = ||u_{ji}^n||$).

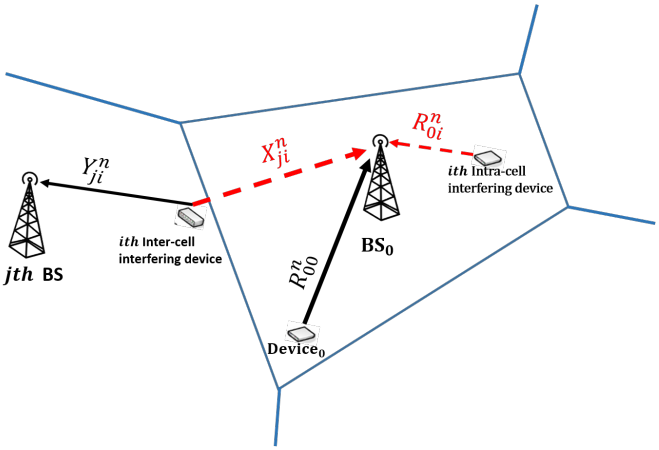

Fig. 2: Link length of inter-cell and intra-cell interfering devices

Let Z denote the distance between any device and its serving BS. Since BSs are distributed according to a PPP with density λ_B and devices are allowed to associate with only one BS at a time, Z has cumulative density function (CDF) given by the void probability of the PPP defined as [21]

$$F_Z(z) = 1 - \exp(-\lambda_B \pi z). \tag{3}$$

Accordingly, from (3), the probability density functions (PDF)s of R_{00}^n, R_{0i}^n and Y_{ji}^n can be shown to follow a Rayleigh distribution defined as [17], [21]

$$f_Z(z) = 2\pi\lambda_B z \exp(-\pi\lambda_B z^2). \tag{4}$$

As for X_{ji}^n, it is possible that an inter-cell interfering device is located closer to BS_0 than some of the devices located inside the Voronoi cell of BS_0. This phenomena is due to the Voronoi tessellation formed by the the spatial abstraction of the BS locations using PPP (see Figure 2). Thus, there is no exact way of differentiating between inter- and intra-cell interfering devices. One way of establishing the segregation is by assuming that a device is inter-cell interfering if at least one BS, other than BS_0, is located within a ball of radius h centered at the device. The probability of this event is the complement of the void probability of the PPP, given by $1-\exp(-\lambda_B\pi h^2)$. Accordingly, the set of inter-cell interfering devices can be spatially modeled using non-homogeneous PPP with density $\lambda_{nI} = \lambda_n(1-\exp(-\lambda_B\pi h^2))$ with respect to the typical BS. Under this assumption, there is no exact distribution for X_{ji}^n [21].

IV. RACH performance analysis

For a device to successfully associate with its desired BS, its transmitted preamble should be received with an SINR above threshold, τ. Let Q_{ji}^n denote the association success probability of the i^{th} device with the j^{th} BS via transmitting the n^{th} preamble. Since preambles are orthogonal, the following analysis is valid for any preamble. Without loss of generality, we focus our analysis on $device_0$ associating with BS_0 located at the origin via transmitting the n^{th} preamble. The association success probability of this typical device is defined as

$$Q_{00}^n = P(\Theta_{00}^n > \tau) = P\left(\frac{P||u_{00}^n||^{(\epsilon-1)\alpha} g_0}{I_{in} + I_{out} + \sigma^2} > \tau\right) \tag{5}$$

As g_0 is exponentially distributed with unity mean, (5) can be written as (see Appendix A)

$$\begin{aligned} Q_{00}^n = E_{||u_{00}^n||}\Big[&\exp\{-\frac{\tau}{P}||u_{00}^n||^{(1-\epsilon)\alpha}\sigma^2\} \\ &\times \mathscr{L}_{I_{in}}\{\frac{\tau}{P}||u_{00}^n||^{(1-\epsilon)\alpha}\}\mathscr{L}_{I_{out}}\{\frac{\tau}{P}||u_{00}^n||^{(1-\epsilon)\alpha}\}\Big] \end{aligned} \tag{6}$$

where $\mathscr{L}_{I_{in}}\{.\}$ and $\mathscr{L}_{I_{out}}\{.\}$ denote the Laplace transforms of intra-cell and inter-cell interference components respectively.

For notational simplicity, let $s = \frac{\tau}{P}||u_{00}^n||^{(1-\epsilon)\alpha}$ such that, given $||u_{00}^n||$, (6) can be rewritten as the conditional success probability given by

$$Q_{00}^n(\tau|u_{00}^n) = \exp\{-s\sigma^2\}\mathscr{L}_{I_{in}}\{s\}\mathscr{L}_{I_{out}}\{s\}. \tag{7}$$

To calculate the Laplace transforms in (7) and find the association success probability, the number of devices in one Voronoi cell needs to be calculated first. Since the number and locations of active devices at the beginning of each transmission *round* are random, the number of devices in each cell is also random. In the following, we derive an approximation for the average number of devices within each Voronoi cell using device density and area of the coverage cell.

A. Average number of devices in a cell

We focus our analysis on BS_0. Let M_0 denote the total number of active devices located in the Voronoi cell of BS_0. Denote $P(M_0 = m)$ as the probability mass function (PMF) of M_0. Since the locations of active devices follow a PPP with density λ_u and the BSs form a Voronoi tessellation, the number of active devices inside the coverage area of any BS follows a conditional Poisson distribution given by [14], [21]

$$P(M_0 = m|V) = \frac{(\lambda_u V)^m e^{-\lambda_u V}}{m!} \tag{8}$$

where V is the area of the Voronoi cell of the BS which is random in nature. The exact distribution of V is not known [21]; however, it can be approximated by a generalized Gamma distribution given by [22]

$$f_V(v;\lambda_B,c) = \frac{\lambda_B^c v^{c-1} e^{-\lambda_B v}}{\Gamma(c)} \tag{9}$$

where $c = 3.575$ is a constant defined for the Voronoi tessellation in $\mathbb{R}^2$ [23] and $\Gamma(c) = \int_0^\infty t^{c-1}e^{-t}\,\mathrm{d}t$. Therefore, the unconditional PMF of M_0 is approximately given by

$$\begin{aligned} P(M_0 = m) &= \int_0^\infty \frac{(\lambda_u v)^m e^{-\lambda_u v}}{m!} f_V(v;\lambda_B,c)\,\mathrm{d}v \\ &\approx \frac{\lambda_B^c \lambda_u^m \Gamma(m+c)}{\Gamma(c)(\lambda_B+\lambda_u)^{m+c} m!}. \end{aligned} \tag{10}$$

Accordingly, the average number of active devices in a Voronoi cell in this network is given by (see Appendix B)

$$\bar{M}_0 = \frac{\gamma\zeta\Gamma(c+1)}{(1-\zeta)^{(c+1)}} \tag{11}$$

where $\gamma = \frac{\lambda_B^c}{\Gamma(c)(\lambda_B+\lambda_u)^c}$ and $\zeta = \frac{\lambda_u}{\lambda_B+\lambda_u}$.

Due to the uniformity of the device distribution, the average number of active devices in the Voronoi cell of any BS is the same, i.e., $\bar{M}_j = \bar{M}_0$ for $j = 1, 2, ...$ For simplicity, we assume that the number of devices in each cell is high enough such that there is at least one device on each preamble. As devices randomly choose the preambles and each preamble is equiprobable to be chosen, we assume that active devices will be divided equally across the N available preambles.

To insure that the number of active devices is integer, define $\bar{M}_j^*$ as the rounded-up average number of active devices in a cell to the nearest multiple of N (i.e., $\bar{M}_j^* = \lceil\frac{\bar{M}_0}{N}\rceil$ for $j = 0, 1, 2, ...$). Accordingly, let $\bar{M}_j^n$ denote the average number of devices interfering on the n^{th} preamble and associated with the j^{th} BS for $j = 0, 1, 2, ...$ and $n = 1, 2, ..., N$. Then, $\bar{M}_j^n$ is given by

$$\bar{M}_j^n = \frac{\bar{M}_j^*}{N} \quad \forall n \; and \; \forall j. \tag{12}$$

Since the average number of devices in each cell is the same and the preambles are equiprobable to be chosen, for simplicity of notation, the superscript and subscript are omitted and thus for the rest of the analysis, we have $\bar{M} = \bar{M}_j^n$ to denote the average number of intra-cell interfering devices on any preamble and associated with any BS. Using the above results, expressions for the Laplace transforms of the interference components in (7) are derived next.

B. Interference Laplace transforms

As a further simplification, we assume that each BS will have exactly $\bar{M}^* = N \cdot \bar{M}$ active devices located within its Voronoi cell at the beginning of each *round*. Although this assumption is dubious, it will help reduce the complexity of the Laplace transforms. The accuracy of this assumption is validated by means of simulations as will be shown in the results section.

Intra-cell interference is due to devices transmitting the same preamble while attempting to associate with the same BS. For device$_0$ associated with BS$_0$, intra-cell interference is a function of the distance from devices located in the Voronoi cell of BS$_0$ to the origin. The Laplace transform of I_{in} is approximately given by (See Appendix C)

$$\begin{aligned}\mathscr{L}_{I_{in}}\{s\} &= E_{I_{in}}[\exp\{-sI_{in}\}] \\ &= E_{g_i,s,||u^n_{0i}||}\left[\exp\{-sP\sum_{u^n_{0i}\in\Psi_{n0}/\{u^n_{00}\}}||u^n_{0i}||^{(\epsilon-1)\alpha}g_i\}\right] \\ &\approx \left(\int_0^\infty \frac{f_{R^n}(r)}{1+sPr^{(\epsilon-1)\alpha}}\mathrm{d}r\right)^{\bar{M}} \end{aligned} \tag{13}$$

where $f_{R^n}(r)$ is the i.i.d PDF of R^n_{0i} (for different i values) given by (4).

Inter-cell interference is due to devices located outside the Voronoi cell of BS$_0$. Inter-cell interfering devices adjust their power to compensate for the path-loss attenuation based on the distances to their serving BSs. For simplicity, assume that the locations of inter-cell interfering devices are modeled by a homogeneous PPP of density λ_n [21]. This assumption is valid when the density of the BSs is high enough, such that the area of the Voronoi cells of each BS becomes very small. With omni-directional antennas, transmissions from inter-cell interfering devices generate interference at BS$_0$. The Laplace transform of the aggregate inter-cell interference is approximately given by (see Appendix D)

$$\begin{aligned}\mathscr{L}_{I_{out}}\{s\} &= E_{I_{out}}[\exp\{-sI_{out}\}] \\ &= E_{g_i,s,||u^n_{ji}-b_j||,||u^n_{ji}||}\left[\exp\{-sP\sum_{j\neq 0}\sum_{u^n_{ji}\in\Psi_{nj}}||u^n_{ji}||^{-\alpha} \right. \\ &\qquad \left. \times ||u^n_{ji}-b_j||^{\epsilon\alpha}g_i\}\right] \\ &= E_{g_i,s,Y^n_{ji},X^n_{ji}}\left[exp\{-sP\sum_{j\neq 0}\sum_{u^n_{ji}\in\Psi_{nj}}(Y^n_{ji})^{\epsilon\alpha}(X^n_{ji})^{-\alpha}g_i\}\right] \\ &\approx \exp\left(-2\pi\lambda_n\int_y^\infty\left[1-\left(\int_0^\infty\frac{f_{Y^n}(y)}{1+sPy^{\epsilon\alpha}x^{-\alpha}}\mathrm{d}y\right)^{\bar{M}}\right]x\,\mathrm{d}x\right) \end{aligned} \tag{14}$$

where $f_{Y^n}(y)$ is the i.i.d PDF of Y^n_{ji} (for different i and j values) given by (4).

Substituting (13) and (14) into (7), the final form of the general conditional success probability, as a function of σ, τ, λ_n, α and ϵ, conditioned on s, is given by

$$\begin{aligned}Q^n_{00}(\sigma,\tau,\lambda_n,\alpha,\epsilon|s) &= \exp\{-s\sigma^2\}\mathscr{L}_{I_{in}}\{s\}\mathscr{L}_{I_{out}}\{s\} \\ &\approx \left[e^{-\left(s\sigma^2+2\pi\lambda_n\int_y^\infty\left[1-\left(\int_0^\infty\frac{f_{Y^n}(y)}{1+sPy^{\epsilon\alpha}x^{-\alpha}}dy\right)^{\bar{M}}\right]xdx\right)}\right. \\ &\qquad \left.\times\left(\int_0^\infty\frac{f_{R^n}(r)}{1+sPr^{(\epsilon-1)\alpha}}\mathrm{d}r\right)^{\bar{M}}\right]. \end{aligned} \tag{15}$$

Since the preceding analysis is applicable to any device-BS pair, let the general association success probability for any device-BS pair be denoted by Q_s. In (15), $s = \frac{\tau}{P}||u^n_{00}||^{(1-\epsilon)\alpha}$ is a function of the random distance $||u^n_{00}||$ between the BS$_0$ and device$_0$. For notational simplicity, let W be the random distance between device$_0$ and BS$_0$ such that W has a PDF $F_W(w)$ given by (4) (i.e. $W = R^n_{00}$). Assuming an interference limited network (i.e. $\sigma = 0$), which is a valid assumption when the number of contending devices is large, the unconditional association success probability as a function of σ, τ, λ_n, α and ϵ is given by (16) shown at the top of the next page.

V. Numerical results and Discussion

In this section, we present numerical results for the association success probability based on (16) and simulations. The association success probability is evaluated versus three major system parameters: density of interfering devices on the n^{th} preamble (λ_n), the power compensation level (ϵ), and the SINR threshold (τ). With the Rayleigh distribution in (4) for Y and R, there is no closed form expression for (16); thus, we resort to numerical calculations that are validated via independent system level simulations. Table II lists the parameters used to obtain the results.

TABLE II. System parameters used to obtain the numerical and simulation results

Parameter	Value	Description
N	64	Number of orthogonal preambles shared by all BSs
P^t_B	43 dBm	Downlink transmission power of any BS
P	1 dBm	Nominal uplink transmission power of any device
α	4	Path-loss attenuation factor
λ_B	1 BS/km^2	Density of BSs
ρ	-65 dBm	Receiver sensitivity of any device
σ	0	Noise variance

Simulations are performed based on the system model in Section II using MATLAB for a 200 km x 200 km 2D plane. Each result is an average of 1000 Monte Carlo simulation runs. In the network, locations of BSs and devices are randomly generated based on their deployment densities. We use 3GPP path-loss model [24] with Rayleigh fading of unit mean. Maximum received signal strength association rule is employed such that a device is associated with the BS from which it receives the highest downlink power. Device receiver sensitivity is set to $\rho = -65$ dBm such that downlink preamble messages received with power less than ρ will not be detected. Devices associated with each BS are then randomly divided into N groups to simulate random preamble generation.

Figure 3 shows the impact of FPC parameter ϵ on the success association probability of the RACH protocol. The results

$$
\begin{aligned}
Q_s &= E_W[Q_{00}^n(\sigma,\tau,\lambda_n,\alpha,\epsilon|W)] \\
&= \int_0^\infty Q_{00}^n(\sigma,\tau,\lambda_n,\alpha,\epsilon,w) f_W(w)\,\mathrm{d}w \\
&= \int_0^\infty Q_{00}^n(\sigma,\tau,\lambda_n,\alpha,\epsilon,w) 2\pi\lambda_B w e^{-\pi\lambda_B w^2}\mathrm{d}w \\
&\approx 2\pi\lambda_B \int_0^\infty w \left[\left(\int_0^\infty \frac{f_{R^n}(r)}{1+\tau w^{(1-\epsilon)\alpha} r^{(\epsilon-1)\alpha}}\mathrm{d}r\right)^{\tilde{M}} e^{-\left(\pi\lambda_B w^2 + 2\pi\lambda_n \int_y^\infty \left[1-\left(\int_0^\infty \frac{f_{Y^n}(y)}{1+\tau w^{(1-\epsilon)\alpha} y^{\epsilon\alpha} x^{-\alpha}}dy\right)^{\tilde{M}}\right] x\mathrm{d}x\right)}\right] \mathrm{d}w. \qquad (16)
\end{aligned}
$$

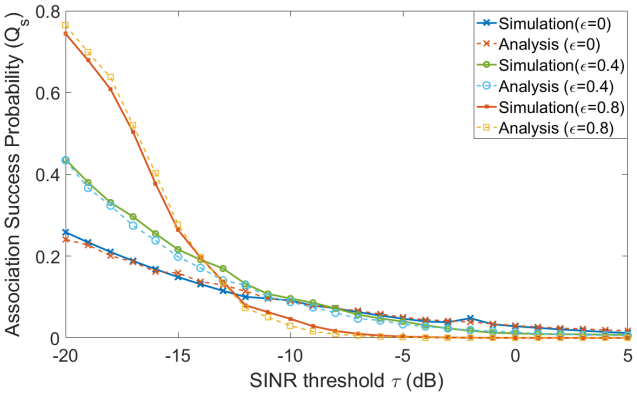

Fig. 3: Uplink association success probability of a typical device transmitting the n^{th} preamble to its serving typical BS

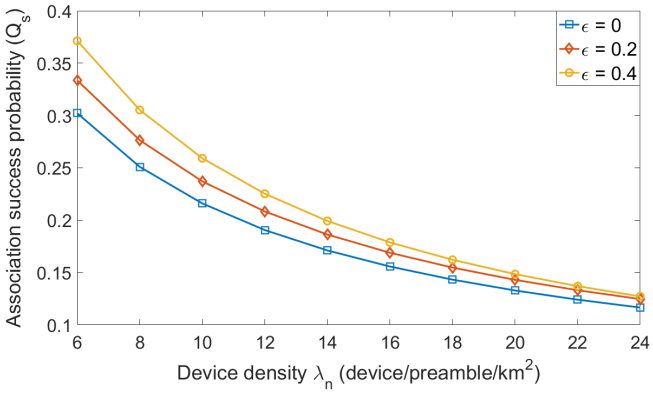

Fig. 4: Effect of increasing device density

are plotted against SINR threshold τ. The FPC parameter is varied between 0 and 0.8 in steps of 0.4. Device density λ_u ($= \lambda_n \cdot N$) is set to be 2560 devices/km^2. As shown in the figure, for all values of ϵ, as threshold τ increases, the success association probability decreases. This behaviour is expected, as fewer devices will be able to achieve high SINR levels due to the extensive interference caused by the high contention. Furthermore, for a low value of τ (< -14 dB), increasing ϵ always results in a higher success association probability. For a larger τ value, the association success probability is almost identical irrespective of ϵ; in fact, a higher ϵ value results in degradation of the success association probability. Note that, the shown results in Figure 3 were obtained at a device density that is respectively high. Accordingly, the results suggest that at high device densities, FPC is beneficial as long as the SINR threshold is low.

Figure 4 shows the relationship between increasing device density and the FPC parameter. The results are obtained by setting $\tau = -5$ dB, and varying device density λ_n between 6 and 24 device/preamble/km^2 in steps of 2. Three ϵ values are studied: 0, 0.2, and 0.4. As shown, for the λ_n values, increasing ϵ results in a higher success probability. However, as λ_n increases, the improvement in success probability associated with FPC decreases as evidenced by the shrinking gap between the curves. Consequently, there is a trade-off between the density of the devices and the gain achieved by employing FPC.

In Figures 3 and 4, to be consistent with the literature, the threshold, τ, varies between -20 dB and 5 dB [10]. While these SINR threshold values may seem somewhat low, we are interested in the trend rather than the actual values. In this work, we study the RACH performance under extreme loading conditions. In fact, λ_n is set to a minimum of 6 indicating that there is at least 6 devices per BS transmitting the n^{th} preamble at the same time. Under such loading conditions, the association success probability at a high SINR value will be extremely low such that the trend will not be visible. In Figure 5, the loading conditions are relaxed by setting λ_n to 2 devices/preamble/km^2. The threshold, τ, varies between -20 dB and 5 dB. As expected, as the device density decreases, the success association probability increases, yet the trend with respect to τ stays the same. Also, the improvement due to FPC is observed.

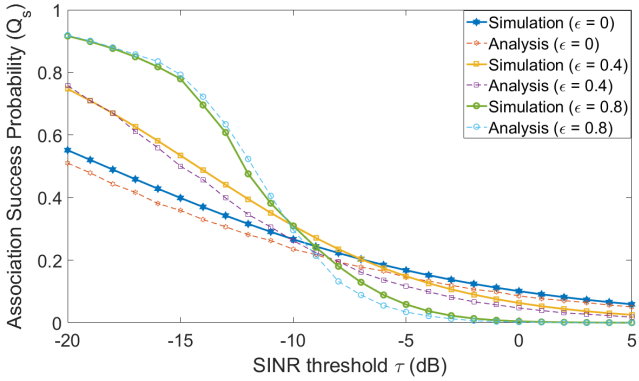

Fig. 5: Association success probability when $\lambda_n = 2$

It is important to note that the number of competing devices changes with time within each *round*. Only a portion of

the active devices will be able to successfully associate in each sub-frame, while the rest will move on to compete in the next sub-frames. This behaviour can be characterized using the association success probability. Let Q_s^f denote the instantaneous (e.g., in the f^{th} sub-frame) association success probability, and λ_u^f denote the progressive density of active devices in the f^{th} sub-frame, which follows the relation

$$\lambda_u^{f+1} = (1 - Q_s^f)\lambda_u^f. \tag{16}$$

Figure 6 shows the association success probability as time progresses (depicted by the number of RAO slots spanned within each *round*). The initial device density per preamble (i.e., λ_n) is set to 30 device/preamble/km^2 (i.e., λ_u = 1920 active device/km^2). The SINR threshold is set at $\tau = -10$ dB and no power control is used (i.e., $\epsilon = 0$). For this parameter setting, devices require 30 RAOs for all of them to successfully associate. This translates into 30 LTE sub-frames, each of length 20ms. This is under the assumptions that devices do not share the LTE-defined 64 preambles with any other applications and that the reception SINR threshold τ is somewhat unrealistically low [6]. In reality however, besides having to target higher and more realistic SINR thresholds, IoT applications will share the available preambles with other more domination human-to-human applications [19]. In fact, many studies advocate dedicating only a small portion of the preambles to IoT applications as a way of avoiding performance degradation of other applications. Having access to a smaller number of preambles leads to even a lower association success probability which translates to a higher access delay. Thus, we can conclude that the RACH protocol is indeed a bottle neck when it comes to supporting a massive number of devices requesting simultaneous access and can potentially hinder the applicability of cellular IoT communication paradigm.

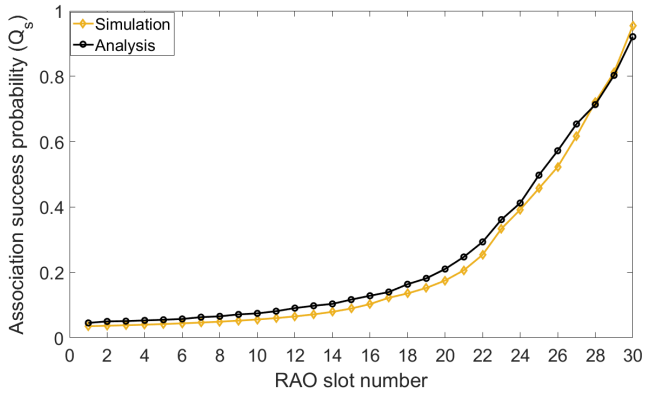

Fig. 6: Association success probability as a function of RAO slot number ($\epsilon = 0$, $\tau = -10$, $\lambda_n = 30$)

Figure 7 shows the impact of FPC on access delay, i.e., the association success probability as time progresses. The device density is set at λ_n = 30 device/preamble/km^2. Two values of the threshold τ are studied: -15 dB and -5 dB. The FPC parameter ϵ is varied between 0 and 0.8 in steps of 0.4. As observed, at a low SINR threshold value, FPC can reduce cellular access delay; while at a high threshold value, besides increasing the energy consumption of the devices, it increases access delay. Consequently, FPC may not be an adequate solution for improving cellular access for the anticipated cellular IoT applications with a massive number of devices, as it results in higher energy wastage, increases access delay and requires operating at an unrealistically low SINR threshold value.

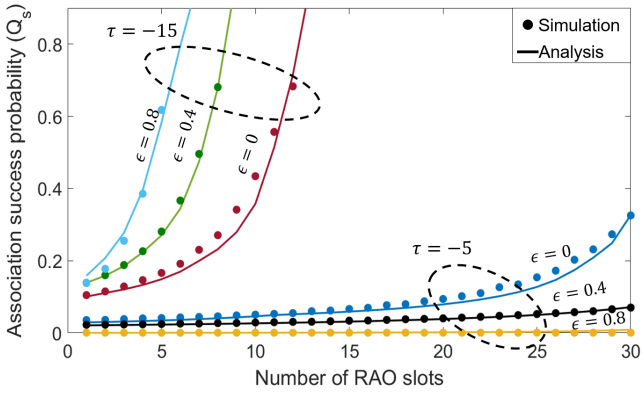

Fig. 7: Association success probability as a function of RAO slot number, ϵ and τ ($\lambda_n = 30$)

In this section, we study the association behavior in cellular networks under a massive number of devices. The derived model for the association success probability of the RACH protocol is analyzed and its accuracy is corroborated via system level simulations. Through extensive simulations, the derived model is shown to be accurate as evident by the close match between the analysis and simulation results. Compared to the models presented in [10], [18], the derived model is more comprehensive and provides the flexibility of analyzing the RACH performance under various situations. For instance, our model can be used to analyze the performance under different path-loss attenuation compensation levels by varying FPC parameter ϵ. Furthermore, other parameters such as device density, number of available preambles, BS density and SINR threshold can be varied to study different network scenarios. Nonetheless, inspired by the work presented in [15], [18], our model can be further generalized into a spatio-temporal model by considering data arrival dynamics at the devices, which is left as a part of our future work.

VI. Conclusion

In this paper, we use stochastic geometry to model the RACH instantaneous association success probability in a single-tier cellular network by modeling the SINR. The objective is to study the access performance of the traditional cellular network when supporting applications with a massive number of devices such as the anticipated IoT. For a device to successfully associate with its desired BS, its RACH association preamble should be received with SINR above a certain threshold. To find the association success probability, we first abstract the network topology by spatially modeling the locations of the BSs and the active devices using two

independent homogeneous PPPs, and then characterize intra-cell interference and inter-cell interference components of the preamble's SINR in the network via deriving expressions for their Laplace transforms. The final model of the SINR is used to find the expression for the association success probability. The model for the association success probability is a function of device density, number of available RACH preambles, BS density, and FPC parameter. The model is corroborated via Monte Carlo simulations conducted using MATLAB. Various network scenarios are tested by using different combinations of the variables in the model. Numerical results demonstrate that there is an advantage of using a power control mechanism as a means for enhancing RACH association probability, particularly when operating at a low SINR threshold value; however, the performance gain decreases as the threshold increases. It is also noticed that, as the number of contending devices decreases, the performance gain due to the employed power control mechanism increases. Considering these observations, we conclude that the limited number of preambles in LTE degrades the access performance as the number of contending devices increases, leading to extensive access delays that may be unacceptable for delay-intolerant IoT applications. Based on the results presented in this study, it is suggested that the current association mechanism of the cellular network may not be adequate for supporting large-scale IoT applications with a massive number of devices, which require ubiquitous energy efficient and delay aware connectivity. Thus, innovative random access should be developed accordingly to efficiently support future IoT applications.

REFERENCES

[1] Q. Ye and W. Zhuang, "Distributed and adaptive medium access control for internet-of-things-enabled mobile networks," *IEEE Internet Things J.*, vol. 4, no. 2, pp. 446–460, Apr. 2017.

[2] A. Rico-Alvarino, M. Vajapeyam, H. Xu, X. Wang, Y. Blankenship, J. Bergman, T. Tirronen, and E. Yavuz, "An overview of 3GPP enhancements on machine to machine communications," *IEEE Commun. Mag.*, vol. 54, no. 6, pp. 14–21, June 2016.

[3] I. Leyva-Mayorga, L. Tello-Oquendo, V. Pla, J. Martinez-Bauset, and V. Casares-Giner, "Performance analysis of access class barring for handling massive M2M traffic in LTE-A networks," in *Proc. IEEE ICC*, May 2016, pp. 1–6.

[4] L. Liang, L. Xu, B. Cao, and Y. Jia, "A cluster-based congestion-mitigating access scheme for massive M2M communications in internet of things," *IEEE Internet Things J.*, vol. 5, no. 3, pp. 2200–2211, June 2018.

[5] D. T. Wiriaatmadja and K. W. Choi, "Hybrid random access and data transmission protocol for machine-to-machine communications in cellular networks," *IEEE Trans. Wireless Commun.*, vol. 14, no. 1, pp. 33–46, Jan. 2015.

[6] ETSI, "LTE; evolved universal terrestrial radio access (E-UTRA); physical channels and modulation (3GPP TS 36.211 version 14.2.0 Release 14)," *TS 36.211 version 14.2.0*, 2017.

[7] M. Gerasimenko, V. Petrov, O. Galinina, S. Andreev, and Y. Koucheryavy, "Energy and delay analysis of LTE-advanced RACH performance under MTC overload," in *Proc. IEEE Globecom Workshops*, Dec. 2012, pp. 1632–1637.

[8] M. Polese, M. Centenaro, A. Zanella, and M. Zorzi, "M2M massive access in LTE: RACH performance evaluation in a smart city scenario," in *Proc. IEEE ICC*, May 2016, pp. 1–6.

[9] G. Y. Lin, S. R. Chang, and H. Y. Wei, "Estimation and adaptation for bursty LTE random access," *IEEE Trans. Veh. Technol.*, vol. 65, no. 4, pp. 2560–2577, Apr. 2016.

[10] M. Gharbieh, H. ElSawy, A. Bader, and M. S. Alouini, "Tractable stochastic geometry model for IoT access in LTE networks," in *Proc. IEEE Globecom*, Dec. 2016, pp. 1–7.

[11] D. Malak, H. S. Dhillon, and J. G. Andrews, "Optimizing data aggregation for uplink machine-to-machine communication networks," *IEEE Trans. Commun.*, vol. 64, no. 3, pp. 1274–1290, March 2016.

[12] M. K. Elhattab, M. M. Elmesalawy, and I. I. Ibrahim, "Opportunistic device association for heterogeneous cellular networks with H2H/IoT co-existence under QoS guarantee," *IEEE Internet Things J.*, vol. 4, no. 5, pp. 1360–1369, Oct. 2017.

[13] N. Jiang, Y. Deng, A. Nallanathan, X. Kang, and T. Q. S. Quek, "Analyzing random access collisions in massive IoT networks," *IEEE Trans. on Wireless Commun.*, vol. 17, no. 10, pp. 6853–6870, Oct. 2018.

[14] R. Zhang, M. Wang, X. Shen, and L. L. Xie, "Probabilistic analysis on QoS provisioning for internet of things in LTE-A heterogeneous networks with partial spectrum usage," *IEEE Internet Things J.*, vol. 3, no. 3, pp. 354–365, June 2016.

[15] M. Gharbieh, H. ElSawy, A. Bader, and M. S. Alouini, "Spatiotemporal stochastic modeling of IoT enabled cellular networks: Scalability and stability analysis," *IEEE Trans. Commun.*, vol. 65, no. 8, pp. 3585–3600, Aug. 2017.

[16] N. Jiang, Y. Deng, X. Kang, and A. Nallanathan, "Random access analysis for massive IoT networks under a new spatio-temporal model: A stochastic geometry approach," *arXiv preprint arXiv:1704.01988*, Apr. 2017.

[17] S. Singh, X. Zhang, and J. G. Andrews, "Joint rate and SINR coverage analysis for decoupled uplink-downlink biased cell associations in HetNets," *IEEE Trans. Wireless Commun.*, vol. 14, no. 10, pp. 5360–5373, Oct. 2015.

[18] N. Jiang, Y. Deng, X. Kang, and A. Nallanathan, "Random access analysis for massive IoT networks under a new spatio-temporal model: A stochastic geometry approach," *IEEE Trans. on Commun.*, pp. 1–16, Jul. 2018.

[19] T. P. C. de Andrade, C. A. Astudillo, and N. L. S. da Fonseca, "Allocation of control resources for machine-to-machine and human-to-human communications over LTE/LTE-A networks," *IEEE Internet Things J.*, vol. 3, no. 3, pp. 366–377, June 2016.

[20] H. ElSawy and E. Hossain, "On stochastic geometry modeling of cellular uplink transmission with truncated channel inversion power control," *IEEE Trans. Wireless Commun.*, vol. 13, no. 8, pp. 4454–4469, Aug. 2014.

[21] M. Haenggi, *Stochastic geometry for wireless networks*, 1st ed. New York, NY, USA: Cambridge University Press, 2012.

[22] M. Ferraro and L. Zaninetti, "On the statistics of area size in two-dimensional thick Voronoi diagrams," *Physica A: Stat. Mech. and its Appl.*, vol. 391, no. 20, pp. 4575–4582, July 2012.

[23] A. Okabe, B. Boots, K. Sugihara, and S. N. Chiu, *Spatial Tessellations: Concepts and Applications of Voronoi Diagrams*. John Wiley & Sons, 2009.

[24] Q. H. Chu, J. M. Conrat, and J. C. Cousin, "Propagation path loss models for LTE-advanced urban relaying systems," in *Proc. IEEE Int. Symp. on Antennas and Propagation (APSURSI)*, July 2011, pp. 2797–2800.